Monocytes maintain central nervous system homeostasis following helminth-induced inflammation

Jianya Peng[a,b,1] , Chandler B. Sy[a,b,1], John J. Ponessa[a,b] , Alexander D. Lemenze[c], Christina M. Hernandez[a,b] , Juan M. Inclan-Rico[a,b] , Arman Sawhney[a] , Hannah G. Federman[a,b], Krupa Chavan[a,b], Vanessa Espinosa[a,d] , Sergei V. Kotenko[a,e], Amariliz Rivera[a,d], and Mark C. Siracusa[a,b,2]

Neuroimmune interactions are crucial for regulating immunity and inflammation. Recent studies have revealed that the central nervous system (CNS) senses peripheral inflammation and responds by releasing molecules that limit immune cell activation, thereby promoting tolerance and tissue integrity. However, the extent to which this is a bidirectional process, and whether peripheral immune cells also promote tolerance mechanisms in the CNS remains poorly defined. Here we report that helminth-induced type 2 inflammation promotes monocyte responses in the brain that are required to inhibit excessive microglial activation and host death. Mechanistically, infection-induced monocytes express YM1 that is sufficient to inhibit tumor necrosis factor production from activated microglia. Importantly, neuroprotective monocytes persist in the brain, and infected mice are protected from subsequent lipopolysaccharide-induced neuroinflammation months after infection-induced inflammation has resolved. These studies demonstrate that infiltrating monocytes promote CNS homeostasis in response to inflammation in the periphery and demonstrate that a peripheral infection can alter the immunologic landscape of the host brain.

neuroimmune cross-talk | helminth | monocyte | innate immune cells

Recent studies have revealed that neuroimmune networks play critical roles in maintaining tissue homeostasis and coordinating host defense to diverse classes of pathogens (1–5). Furthermore, a growing body of literature suggests that neuroimmune cross-talk is necessary to limit immune cell activation and promotes tolerance mechanisms needed to maintain the integrity of affected tissues (2, 6–9). Additionally, the nervous system can initiate an anti-inflammatory reflex that inhibits the production of proinflammatory cytokines, such as tumor necrosis factor (TNF), to avoid the development of potentially lethal inflammation (10, 11). However, whether infiltrating immune cells play similar roles by regulating inflammatory responses and homeostasis in the central nervous system (CNS) following the induction of peripheral inflammation remains poorly defined.

Helminth parasites represent some of the most prevalent pathogens worldwide and have infected humans for millennia (12, 13). *Trichinella spiralis*, the causative agent of trichinellosis, is one of several species of *Trichinella* that infects an extremely broad range of hosts, including mammals, birds, and reptiles (14). As a result of these zoonotic qualities, trichinellosis is one of the most successful and widespread parasitic infections in the world (15). *Trichinella* has been detected in the mummified remains of Egyptians and was thought to have been contracted by early hominids during the Pliocene or early Pleistocene Epoch (16, 17). Therefore, like many helminth parasites, *Trichinella* and humans have coevolved and as a result have developed complex host–parasite relationships that involve multiple body systems (18–20).

Protective responses to helminth parasites require the simultaneous induction of inflammation needed to promote worm expulsion and tolerance mechanisms required to prevent excessive tissue damage (12, 13, 21). By studying helminth infections, we have gained invaluable insight into the regulatory mechanisms required to prevent pathologic inflammation and maintain the integrity of affected tissues (2, 4–8, 22, 23). This work has dramatically informed our understanding of the development and actions of alternatively activated or M2 macrophages that play essential roles in promoting tolerance in the context of antihelminth immunity (21, 24–26). Furthermore, our work and that of others have also demonstrated that neuroimmune interactions serve to limit immune cell activation and are required to prevent helminth-induced immunopathology in the lung and gut (6–8). Despite these advances, the immunologic and neuroimmune pathways that promote tolerance mechanisms in peripheral tissues in response to many parasitic helminths remain poorly defined. Additionally, whether

Significance

Neuroimmune networks play critically important roles in coordinating host defense to diverse pathogens. Furthermore, a growing body of literature suggests that neuroimmune cross-talk limits immune cell activation and thereby promotes the integrity of peripheral tissues. However, whether this is a bidirectional process and immune cells play similar roles by regulating inflammatory responses and homeostasis in the central nervous system (CNS) remains poorly defined. Here we report that helminth-induced type 2 inflammation promotes monocyte responses in the brain that are required to inhibit excessive microglial activation and host death. This work defines the ability of infiltrating monocytes to promote CNS homeostasis in the context of peripheral inflammation and highlights bidirectional and previously unappreciated aspects of neuroimmune cross-talk.

these neuroimmune interactions are bidirectional and also involve immune cells infiltrating into the CNS to prevent potentially lethal neuroinflammation remains unknown.

Here we demonstrate that mice infected with *T. spiralis* suffer from rapid weight loss and mortality following monocyte depletion despite having equivalent parasitic burdens. Monocyte-depleted mice showed no evidence of intestinal barrier defects, liver failure, or altered kidney function following infection. Rather, *T. spiralis*-infected mice depleted of monocytes exhibited enhanced microglial activation, elevated expression of proinflammatory cytokines in the brain, and increased cachexia-like disease. Importantly, brain-infiltrating monocytes expressed immunoregulatory factors that are induced independently of type 2 cytokine signaling and are sufficient to inhibit infection-induced microglia. Consistent with a long-term effect, neuroprotective monocytes persisted in the CNS after peripheral inflammation was resolved, and infected mice were significantly protected from subsequent lipopolysaccharide (LPS)-induced neuroinflammation. These data suggest that helminth-induced inflammation is sufficient to fundamentally alter the immunologic landscape of the host brain. This work defines the ability of infiltrating monocytes to promote CNS homeostasis in the context of peripheral inflammation and highlights bidirectional and previously unappreciated aspects of neuroimmune cross-talk.

Results

CCR2⁺ Monocytes Are Required for Survival Post-*T. spiralis* Infection. Previous studies have established that several different cellular and molecular mechanisms promote host tolerance and thereby prevent immunopathology in the context of helminth infections (27, 28). Included among these are the actions of M2 macrophages and neuroimmune regulatory circuits (2, 6, 8, 22, 23, 26). Despite these advances, the pathways that promote tolerance following *T. spiralis* infection, one of the most widely spread parasitic infections in the world, remain to be defined. Therefore, we first sought to investigate the actions of M2 macrophages during the intestinal phase of *T. spiralis* infection. Eight days post-infection (dpi), expression of the M2-associated markers *Arg1*, *Retnla*, and *Chil3* were increased in the small intestine, suggesting the presence of infection-induced M2s (Fig. 1*A*). To evaluate the contributions of macrophages to host protection, we treated mice with phosphate buffered saline- (PBS) or clodronate-loaded (CL) liposomes intravenously post-infection to deplete various myeloid cell populations (29). As expected, both Ly6C⁺CD11b⁺ monocytes and F4/80⁺CD11b⁺ macrophages were depleted in response to CL liposome treatment (Fig. 1 *B*–*E*). Furthermore, CL liposome treatment resulted in the loss of infection-induced expression of *Arg1*, *Retnla*, and *Chil3* in the small intestine (Fig. 1*A*). No significant changes in *iNOS* expression were observed between infected animals regardless of PBS or CL treatment (*SI Appendix*, Fig. S1*A*). Critically, mice treated with CL liposomes exhibited increased weight loss and mortality compared to control mice (Fig. 1 *F* and *G*). These data demonstrate that depletion of phagocytic cells via CL liposome delivery results in the loss of infection-induced M2 responses in the intestine, which is associated with increased host morbidity and mortality.

Intestinal macrophages are primarily derived from C-C chemokine receptor type 2⁺ (CCR2⁺) Ly6C⁺ monocytes that have migrated from the bone marrow (30). Although monocytes are known to make important contributions to the development of protective immunity against pathogens, including bacteria, viruses, and fungi, their contributions to antihelminth responses remain

less defined (31). To test whether monocytes are recruited to the gut following a *T. spiralis* infection, we utilized a CCR2-GFP reporter mouse model and analyzed cellular responses in the intestine via flow cytometric analysis (32). Significant increases in CCR2⁺ monocytes could be detected in the small intestine post-infection (Fig. 2 *A* and *B*). While the CL-based studies above were sufficient to deplete monocytes, liposome treatment is nonspecific and can be toxic if given in high enough doses (33). Therefore, we employed a highly selective diphtheria toxin (DT)-based system in which CCR2⁺ cells can be depleted following administration of DT (CCR2-DTR mice) (34). Consistent with our CL liposome-based studies, depletion of CCR2⁺ monocytes following DT treatment resulted in significantly reduced expression of *Arg1*, *Retnla*, and *Chil3* in the gut (Fig. 2*C*), and increased morbidity and mortality (Fig. 2 *D* and *E*). Collectively, these data suggest that monocytes are critical for host survival following *T. spiralis* infection.

The data presented above provoke the hypothesis that monocytes promote survival following helminth infection by contributing to protective M2 responses in the intestine. M2s are known to promote host protection via their ability to limit parasite burden and maintain the integrity of affected tissues (23, 35–37). Therefore, we first sought to evaluate if mice depleted of CCR2⁺ monocytes showed differences in worm burden and intestinal inflammation. Surprisingly, monocyte-depleted mice exhibited equivalent parasite burdens and similar intestinal pathology as control mice (Fig. 2 *F* and *G*). Furthermore, no significant differences in plasma endotoxin levels were detected following monocyte depletion, and serum levels of C-reactive protein (Crp), a marker of septic shock, were also found to be unchanged between infected mice and controls; suggesting that the barrier integrity of the intestinal tract of monocyte-depleted mice remains unchanged (Fig. 2 *H* and *I*). These interesting results suggest that monocytes promote host survival in a manner that is not directly connected to their ability to support protective responses at the host–parasite interface in the gastrointestinal tract.

Type 2 Cytokine Responses and Adaptive Immunity Are Not Required for Host Survival Post-*T. spiralis* Infection. It is well-established that type 2 cytokine responses are critically important for limiting parasite burden and preventing tissue damage following a helminth infection (38–40). Our data illustrate that the loss of CCR2⁺ bone marrow-derived monocytes results in reduced expression of M2-associated markers in the gut (Fig. 2*C*), as well as increased morbidity and mortality (Fig. 2 *D* and *E*). However, our finding of equivalent parasite burdens and similar intestinal pathology in monocyte-depleted and control mice suggested that monocytes might be contributing to host protection independently of supporting M2s. To further evaluate this possibility, we utilized signal transducer and activation of transcription 6 (STAT6) knockout (KO) mice to evaluate whether type 2 cytokine signaling is required for host survival following infection (41). As expected, *T. spiralis*-infected STAT6KO mice exhibited reduced production of interleukin 4 (IL-4) (*SI Appendix*, Fig. S1*B*), reduced immunoglobulin (Ig) E levels (*SI Appendix*, Fig. S1*B*), diminished expression of M2-associated markers in the gut (*SI Appendix*, Fig. S1*C*), and suffered from significantly increased worm burdens compared to controls (*SI Appendix*, Fig. S1*D*). However, despite dramatically increased worm burdens, STAT6KO animals maintained normal weight and showed no infection-induced mortality, suggesting that the increased mortality exhibited by monocyte-depleted mice is uncoupled from parasite load (*SI Appendix*, Fig. S1 *E* and *F*). Similar to STAT6KO animals, *T. spiralis*
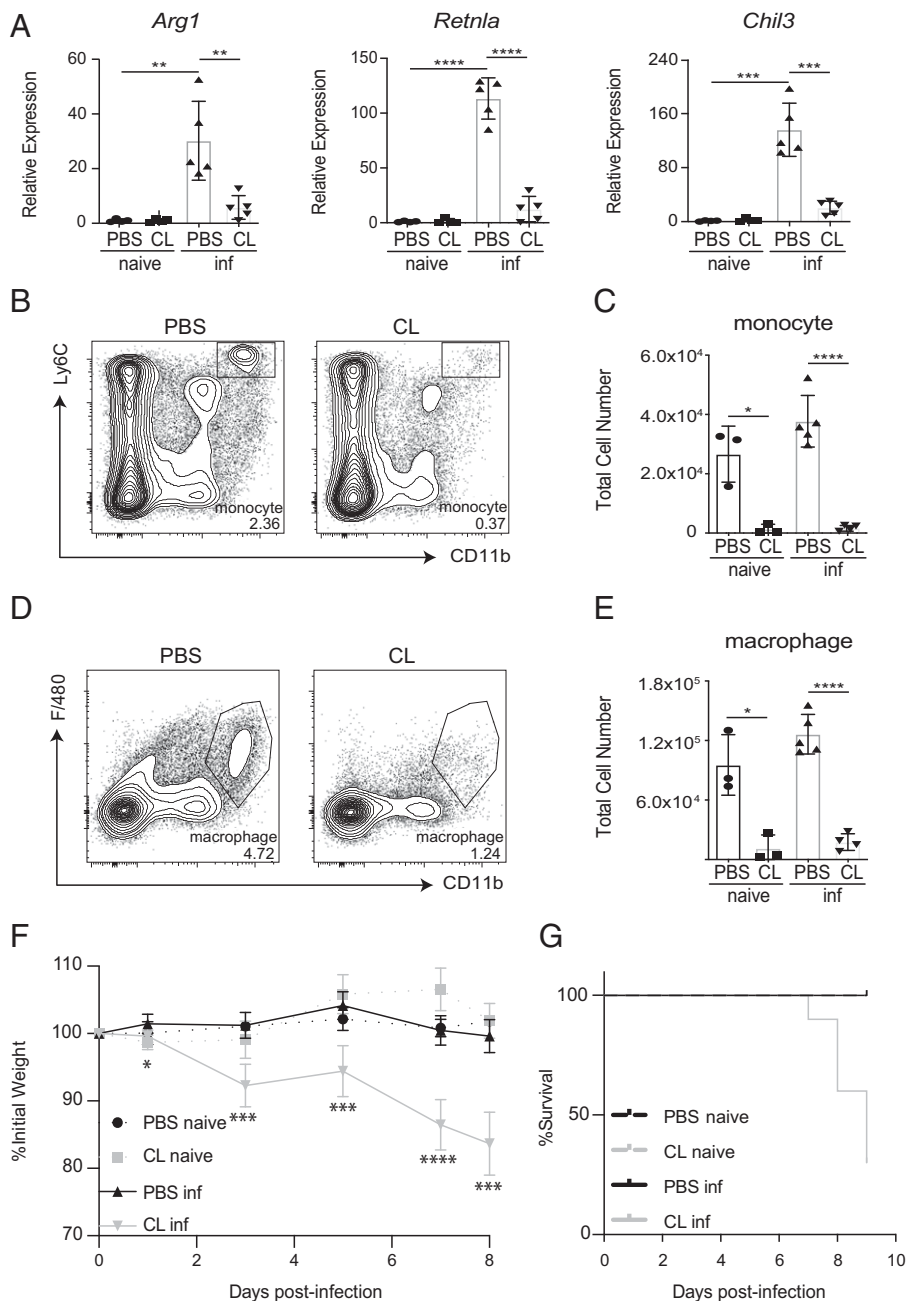
Fig. 1. Loss of M2 macrophages is associated with increased morbidity and mortality post-*T. spiralis* infection. Mice treated with PBS- or clodronate-loaded (CL) liposomes intravenously were infected with *T. spiralis* and sacrificed on 8 days post-infection (dpi). (*A*) Intestinal expression of M2-associated markers was evaluated via RT-qPCR. The presence or absence of (*B* and *C*) monocytes (Ly6C$^+$CD11b$^+$) and (*D* and *E*) macrophages (F4/80$^+$CD11b$^+$) in the spleen was determined via flow cytometry. Populations are gated from CD45^{hi}CD3$^-$CD19$^-$Ly6G$^-$ cells. Numbers in cytometry plots represent the percentage of CD45^{hi} cells. (*F*) Weights and (*G*) mortality were tracked throughout the course of the infection. All panels are representative of at least three independent experiments with at least three biological replicates per group per experiment. Statistical analysis was performed using Student's *t* test. *$P < 0.05$; **$P < 0.01$; ***$P < 0.001$; ****$P < 0.0001$. For (*F*), statistics are comparing CL inf group to PBS inf group for each day. Error bars represent ± SD. inf, *T. spiralis*-infected.

infected Rag2-deficient mice also maintained normal weights and showed no increase in infection-induced mortality (*SI Appendix,* Fig. S1 *G* and *H*). Collectively, these data provoke the hypothesis that monocytes promote host protection independently of a type 2 cytokine responses and adaptive immunity that are known to play critical roles in promoting host tolerance in peripheral tissues (21, 42–45).

Loss of CCR2$^+$ Monocytes Results in Infection-Induced Neuro-inflammation. Monocyte-depleted mice infected with *T. spiralis* succumb to infection within 8 to 10 dpi (Fig. 2*E*). The lack of severe pathology in the gastrointestinal tract prompted us to investigate abnormalities in other organs. We first investigated whether there were alterations in the liver and kidneys of monocyte-depleted mice, as overly robust inflammatory responses in the periphery can damage these organs and has been shown to cause acute mortality in other models (46–49). Importantly, expression levels of IL-1β (*Il1b*) and *Crp*, well-defined markers of liver

inflammation, were found to be at baseline levels in monocyte-depleted mice (*SI Appendix,* Fig. S2*A*) (50). Consistent with these results, alanine aminotransferase levels, an established marker for liver cell injury, were also found to be normal, and no obvious liver pathology was observed in infected mice regardless of monocyte depletion (*SI Appendix,* Fig. S2 *B* and *C*). Moreover, monocyte-depleted mice did not exhibit increased expression of the injury-associated markers *Il-18* and hepatitis A virus cellular receptor 1 (*Havcr1*) in the kidneys following infection (*SI Appendix,* Fig. S2*D*) (51). Furthermore, no significant changes in serum creatine kinase levels, an established marker of kidney injury, or kidney pathology, were detected in monocyte-depleted mice (*SI Appendix,* Fig. S2 *E* and *F*). Collectively, these data suggest that the increased morbidity and mortality seen in monocyte-depleted mice is not the result of unchecked cytokine production or tissue damage occurring in the periphery.

In addition to M2 macrophages, it is now appreciated that neuroimmune interactions play critically important roles in
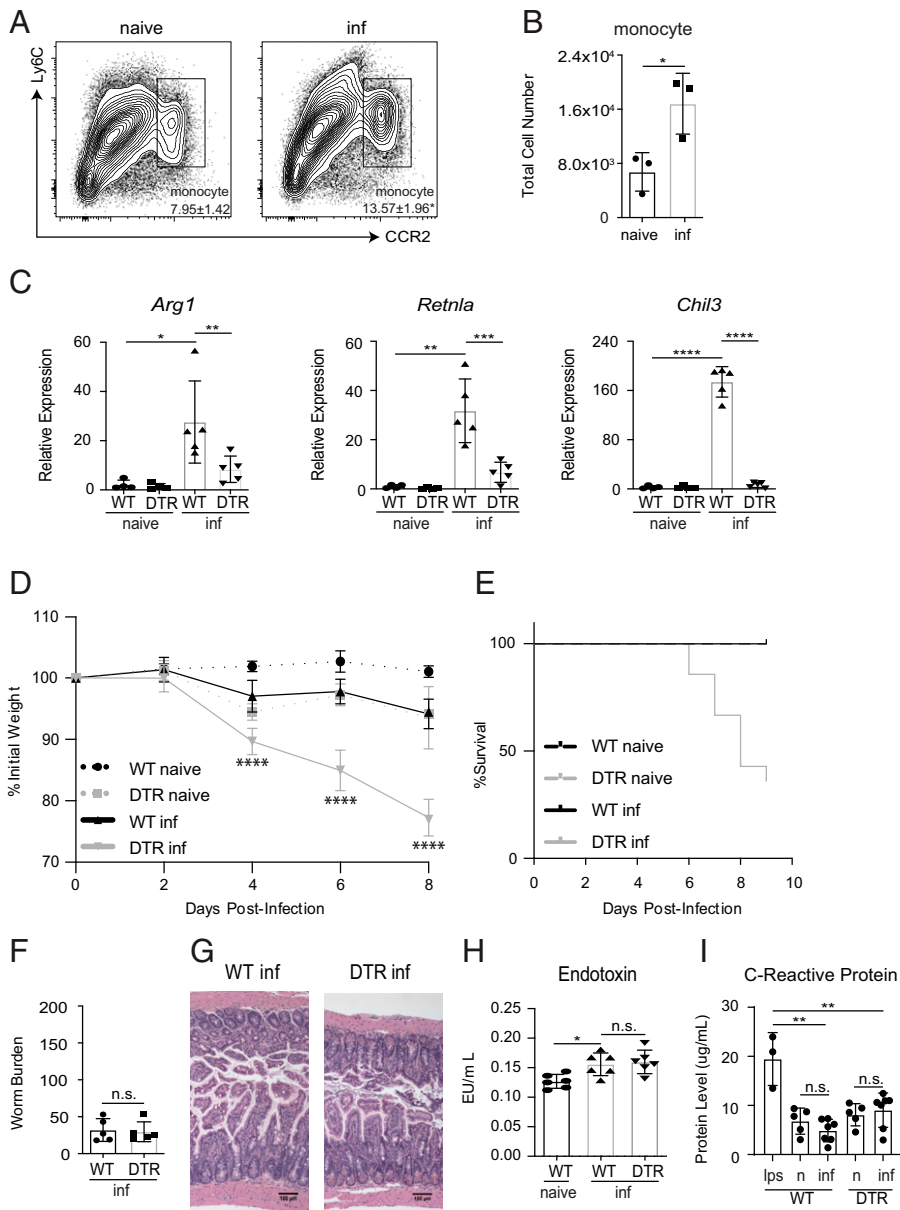
Fig. 2. CCR2+ monocytes are required for survival after *T. spiralis* infection. CCR2-GFP mice were infected with *T. spiralis*. On 8 dpi, small intestine tissue was made into a single-cell suspension and (*A*) the percent (gated on CD45hiEpCAM− cells) and (*B*) total cell number of CCR2+ monocytes were determined via flow cytometry. Numbers in cytometry plots represent the percentage of CD45hiEpCAM− cells. WT or CCR2-DTR (DTR) mice were treated with diphtheria toxin (DT) intraperitoneally (i.p.) every other day and sacrificed 8 dpi. (*C*) Intestinal expression of M2-associated markers was evaluated via RT-qPCR. (*D*) Weights and (*E*) mortality were tracked throughout the course of the infection. (*F*) Worm burden, (*G*) H&E staining of intestinal tissue, (*H*) plasma endotoxin levels, and (*I*) Crp levels were evaluated on 8 dpi. All panels are representative of at least three independent experiments with at least three biological replicates per group per experiment. Statistical analysis was performed using Student's *t* test. *$P < 0.05$; **$P < 0.01$; ***$P < 0.001$; ****$P < 0.0001$; n.s., not significant. For (*D*), statistics are comparing WT-infected group to DTR-infected group. Error bars represent ± SD. inf, *T. spiralis*-infected. n, naive.

promoting tolerance mechanisms in the context of antihelminth immunity (2, 6, 8, 27). Consistent with the possible involvement of the nervous system, previous clinical studies have described a small subset of patients suffering from trichinellosis that exhibit substantial neurological deficits and increased infection-induced death (52). Therefore, we sought to determine whether monocyte-depleted mice exhibit infection-induced changes in the CNS. To investigate this, we performed RNA-sequencing (RNA-seq) on whole-brain tissue taken from groups of naive or infected control and monocyte-depleted mice. RNA-seq analysis revealed that infected monocyte-depleted mice exhibit substantially altered gene expression patterns compared to both naive and infected control mice (Fig. 3*A* and *SI Appendix,* Table S1). Specifically, infected mice depleted of monocytes presented with significantly increased expression of proinflammatory genes—including *Tnf, Nlrp3, Il1b,* and *Il12b*—compared to controls (Fig. 3*A* and *SI Appendix,* Table S1).

Consistent with these changes, gene set enrichment analysis (GSEA) revealed that the brains of infected monocyte-depleted mice were enriched for expression patterns associated with TNF-mediated signaling (Fig. 3*B* and *SI Appendix,* Fig. S3*A*).

It is well established that TNF expression in the brain can have devastating consequences. For example, it has been demonstrated that TNF contributes to neurodegeneration in multiple sclerosis, Alzheimer's disease, Parkinson's disease, and amyotrophic lateral sclerosis, and can also cause cachexia or wasting disease that results in acute death (53–56). Therefore, to further confirm the increased expression levels of *TNF* and other proinflammatory cytokines, we performed quantitative reverse-transcription PCR (RT-qPCR) analysis on the brains of control and monocyte-depleted mice. Substantiating our RNA-seq analysis, *Tnf, Il1b,* and *Il6* were found to be expressed at significantly higher levels in the brains of *T. spiralis*-infected monocyte-depleted mice compared to controls (Fig. 3 *C–E* and *SI Appendix,* Fig. S3*B*). Interestingly, there was also a milder but significant increase in *Tnf* and *Il1b* expression in infected WT mice compared to naive controls, suggesting that there is an attenuated proinflammatory signature in the brains of monocyte-sufficient mice following infection. Importantly, this proinflammatory signature remained suppressed in the brains of infected STAT6KO mice, further supporting that inflammation in the brain is occurring independently of increased worm
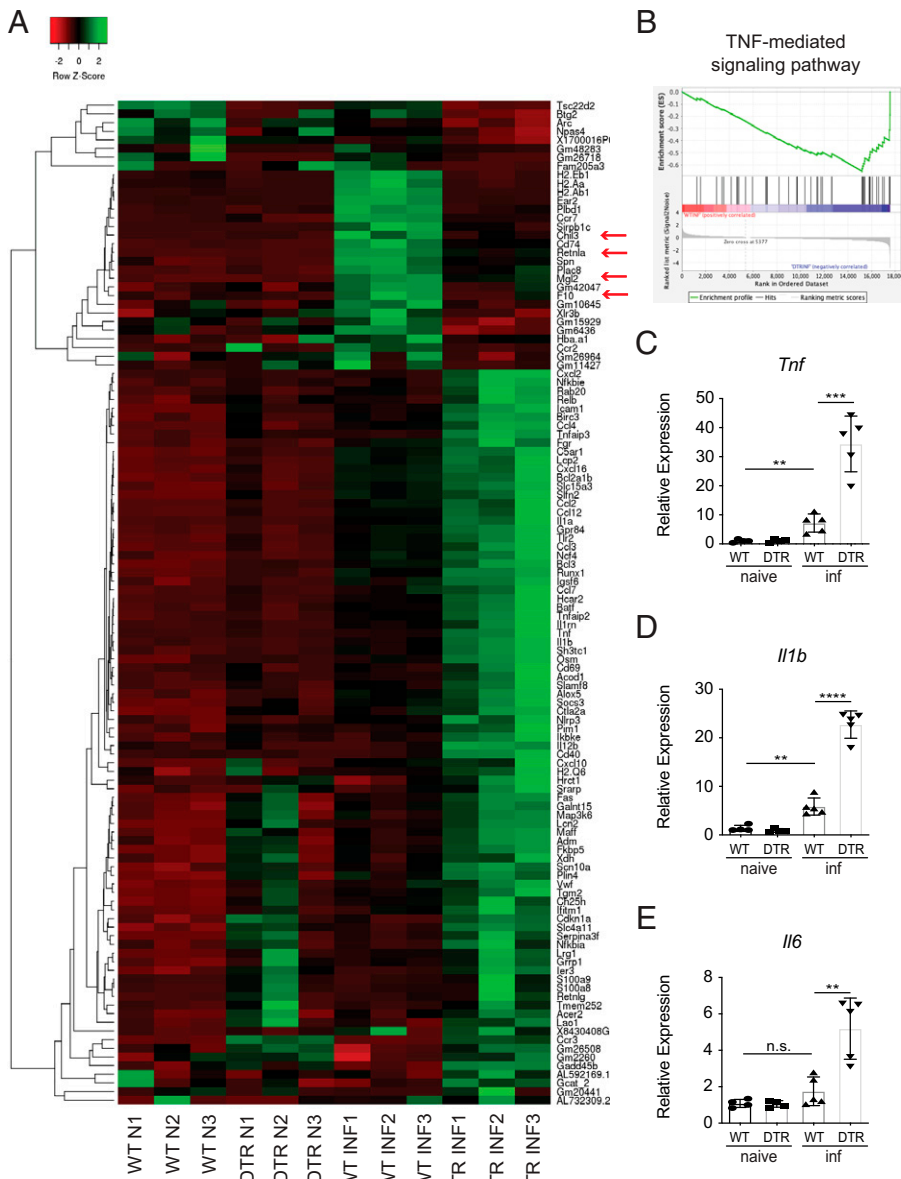
Fig. 3. Loss of CCR2$^+$ monocytes results in a proinflammatory signature in the brain. WT and CCR2-DTR (DTR) mice were infected with *T. spiralis* and treated with DT (i.p.) every other day. Mice were sacrificed 8 dpi. (*A*) Heat map includes genes that are upregulated (FC > 1.5) or downregulated (FC < −1.5) in infected WT versus infected DTR mice and includes three biological replicates per naive group (N) and three biological replicates per infected group (INF). (*B*) GSEA for TNF-mediated signaling pathway. (*C*–*E*) RNA from brain tissue was extracted, and expression of proinflammatory-associated markers was evaluated via RT-qPCR. *C*–*E* are representative of at least three independent experiments with at least three biological replicates per group per experiment. Statistical analysis was performed using Student's *t* test. **$P < 0.01$; ***$P < 0.001$; ****$P < 0.0001$; n.s., not significant. Error bars represent ± SD. inf, *T. spiralis*-infected.

burdens or a loss of protective type 2 cytokine signaling (Fig. 4*A* and *SI Appendix*, Fig. S3*C*). Next, we sought to determine if similar increases in TNF could also be detected in the periphery of monocyte-depleted mice. Importantly, plasma levels of TNF remained similar to WT levels regardless of infection or monocyte-depletion (*SI Appendix*, Fig. S3*D*). These data are consistent with our Crp results (*SI Appendix*, Fig. S2*A*) and suggest that the increased morbidity and mortality observed in infected monocyte-depleted mice is not occurring because of proinflammatory cytokine production in the periphery.

Since the expression of TNF in the CNS is reported to cause cachexia and death, we sought to investigate if a loss of TNF signaling would have a protective effect on infected monocyte-depleted mice (57). To test this, we crossed TNFKO mice with CCR2-DTR mice to generate mice that could be depleted of monocytes in a TNF-deficient environment (58). As expected, infection-induced TNF expression was abolished in the brains of TNFKO mice following monocyte-depletion (*SI Appendix*, Fig. S3*D*). Critically, we found that TNFKO mice depleted of monocytes were significantly protected from infection-induced weight loss compared to TNF-sufficient controls (Fig. 4*B*). These

experiments strongly suggest that expression of TNF in the CNS contributes to poor outcomes observed in monocyte-depleted mice.

It is well-established that neural inflammation in the CNS can alter microglial morphology (59). Therefore, we utilized immunofluorescence microscopy to stain brain sections for the ionized calcium binding adaptor molecule 1 (IBA1) that is used to assess the activation state of microglia. Microglia from infected control and monocyte-depleted mice exhibited intensified expression of IBA1 compared to their naive counterparts, indicating that microglia from both groups respond to infection (Fig. 4*C*) (59). We also investigated expression levels of CD68 on microglia as a general marker for activation. Consistent with infection-induced activation, the percent of microglia expressing CD68 was significantly increased in infected animals compared to naive controls (*SI Appendix*, Fig. S3*F*). To better determine their activation status, we sort-purified microglia (CD45^{mid} CD11b$^+$ cells) (*SI Appendix*, Fig. S3*G*) from naive or infected control and monocyte-depleted mice and measured their cytokine expression levels (60, 61). We found that microglia isolated from infected monocyte-depleted mice expressed
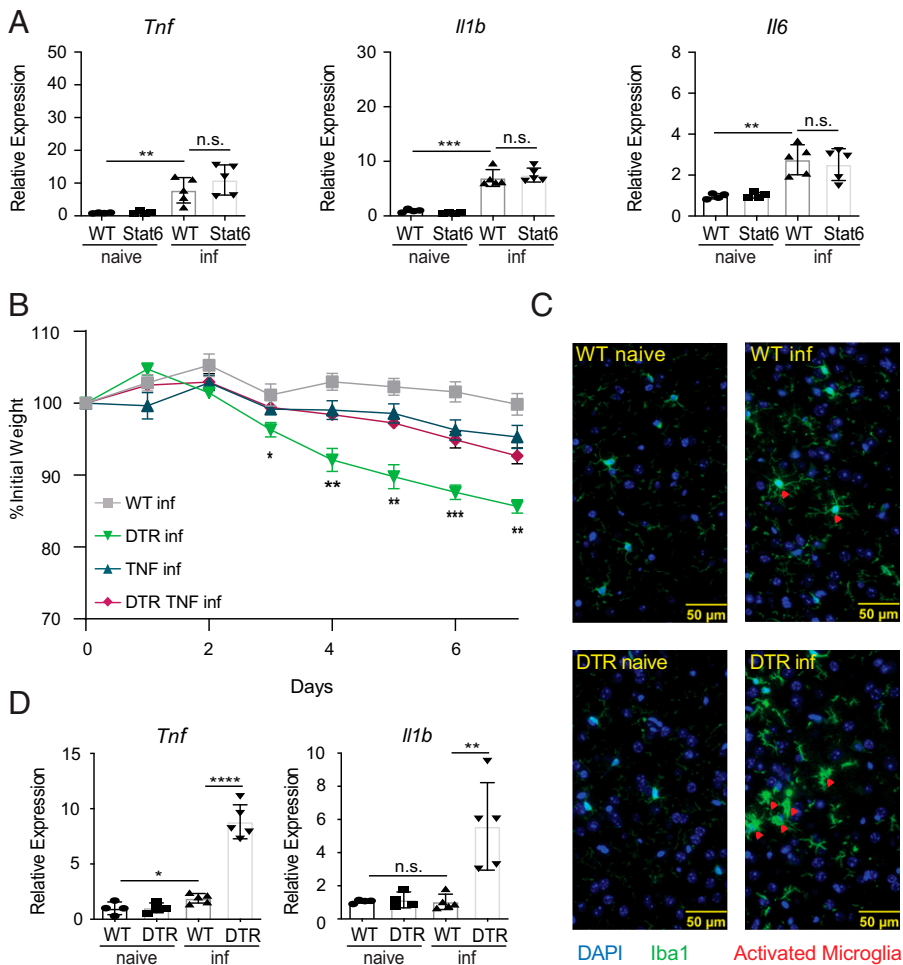
Fig. 4. CCR2$^+$ monocytes limit production of proinflammatory cytokines in the brain post-*T. spiralis* infection. (*A*) RNA from WT or STAT6KO (Stat6) mice brain tissue was extracted, and expression of proinflammatory-associated markers was evaluated via RT-qPCR. WT, DTR, TNF KO (TNF), and CCR2-DTR/TNF KO (DTR TNF) mice were treated with DT (i.p.) every other day and sacrificed 8 dpi. (*B*) Weights were tracked throughout the course of the infection. (*C*) Brains were taken from WT or DTR-infected mice 8 dpi, sectioned, and co-stained with anti-ionized calcium-binding adaptor protein-1 (anti-IBA1) and 4′,6-diamidino-2-phenylindole (DAPI). Red arrowheads indicate activated microglia from the brains of infected mice. (*D*) Microglia (CD45^{mid}CD11b$^+$) were sort-purified from naive and infected WT or DTR mice, and expression of proinflammatory-associated markers was evaluated via RT-qPCR. All panels are representative of at least three independent experiments with at least three biological replicates per group per experiment. Statistical analysis was performed using Student's *t* test. *P < 0.05; **P < 0.01; ***P < 0.001; ****P < 0.0001; n.s., not significant. For (*B*), statistics are comparing DTR-infected to DTR TNF-infected. Error bars represent ± SD. inf, *T. spiralis*-infected.

significantly higher levels of *TNF* and *IL-1β* than those isolated from infected WT mice (Fig. 4*D*). Collectively, these data suggest that monocytes promote CNS homeostasis by limiting infection-induced proinflammatory cytokine expression by microglia.

Expression of Proinflammatory Cytokines in the Brain Is Associated with Muscle Atrophy. The proinflammatory signature observed in the brains of monocyte-depleted mice is likely the cause of the increased infection-induced morbidity and mortality. Neuroinflammation can induce loss of appetite, which is modulated by the appetite-associated hormones leptin and ghrelin (62). However, no significant differences in leptin or ghrelin were observed following monocyte depletion (*SI Appendix*, Fig. S4 *A* and *B*). It has previously been reported that the expression of proinflammatory cytokines in the brain can result in muscle atrophy, that leads to severe weight loss and death (57). Therefore, to determine whether monocyte-depleted mice presented with these characteristics of brain inflammation, we evaluated the expression of markers associated with atrophy in the gastrocnemius muscle. While we did not observe any significant differences in the expression of *Tnf* in the muscle (*SI Appendix*, Fig. S4*C*), monocyte-depleted mice exhibited significantly higher expression of the atrophy-associated markers atrogin-1, muscle RING finger-1 (*MuRF1*), and forkhead box O (*Foxo*)*1* compared to control mice (*SI Appendix*, Fig. S4*D*) (63, 64). Moreover, investigation of the gastrocnemius muscle from infected monocyte-depleted mice revealed that their muscle fibers had significantly reduced cross-sectional areas compared to the fibers of infected

WT mice (*SI Appendix*, Fig. S4 *E* and *F*). Consistent with an important role for TNF in promoting infection-induced morbidity, no differences in cross-sectional areas were observed in TNFKO mice depleted of monocytes compared to control mice (*SI Appendix*, Fig. S4*G*). These data suggest that monocytes activated in the periphery support host protective responses by promoting homeostasis in the CNS that is required to prevent infection-induced cachexia.

Monocyte Populations Are Increased in the Brain Following a *T. spiralis* Infection and Express Immunoregulatory Factors. Our data suggest that monocyte depletion results in increased weight loss and mortality due to brain inflammation and muscle atrophy post-infection. However, whether monocytes increase their presence in the brain post-infection remains unknown. To address this, we first investigated the expression of the chemo-attractive protein C-C motif chemokine ligand 2 (CCL2) that is known to promote monocyte recruitment (65). Significant increases in *Ccl2* expression were detected in the brains of infected mice regardless of monocyte depletion (*SI Appendix*, Fig. S5*A*). Next, we sort-purified microglia from the brains of control and infected groups of mice and found that the microglia from infected animals also expressed significantly higher levels of *Ccl2* than those isolated from uninfected controls (*SI Appendix*, Fig. S5*B*). Interestingly, infection-induced *Ccl2* was found to be expressed at significantly higher levels in microglia from monocyte-depleted mice compared to infected controls (*SI Appendix*, Fig. S5*B*). Collectively, these data provoke the hypothesis that

T. spiralis-induced monocytes are being recruited to the brain, in part, through the contributions of activated microglia. To further evaluate the presence of cellular infiltrates, we performed flow cytometric analysis and assessed the composition of *T. spiralis*-induced cell populations in the brain. There were significant increases in the percent and number of monocytes (*SI Appendix*, Fig. S5 *C* and *D*), macrophages (*SI Appendix*, Fig. S5 *E* and *F*), and dendritic cells (*SI Appendix*, Fig. S5 *G* and *H*) in the brains of infected mice compared to naive controls (*SI Appendix*, Fig. S5 *C–H*). Furthermore, these populations were significantly reduced in CCR2-DTR mice treated with DT post-infection (*SI Appendix*, Fig. S5 *C–H*). These data suggest that monocytes migrate to the brain post-infection, where they can differentiate into macrophages and dendritic cells, and that these populations can be successfully depleted by targeting CCR2.

To further investigate the functions of monocytes and their derived cells, we performed single-cell RNA-seq on sort-purified

CD45^{hi} cells from the brains of naive control, infected control, and infected CCR2-DTR mice. t-Distributed stochastic neighbor embedding (t-SNE) dimension reduction was utilized to visualize distinct immune cell populations in the brain (Fig. 5 *A* and *B*). Ten distinct cell clusters were identified, and populations 4 and 5 were found at increased proportions post-infection but were substantially reduced following DT treatment (Fig. 5 *A* and *B*). These data suggest that these clusters represent monocytes and monocyte-derived macrophages/dendritic cells. Consistent with these observations, CCR2 was a marker gene expressed by cluster 4, and major histocompatibility complex (MHC) II was a marker gene of cluster 5 (Fig. 5*A*). Importantly, clusters 4 and 5 were also defined by the expression of the M2-associated markers *Mgl2*, *Retnla*, and *Chil3*, which are reported to mitigate tissue damage (23, 66, 67). Furthermore, clusters 4 and 5 also expressed the coagulation factor X (*F10*), which is known to be produced in the context of systemic inflammation and has been shown to possess immunomodulatory properties including the
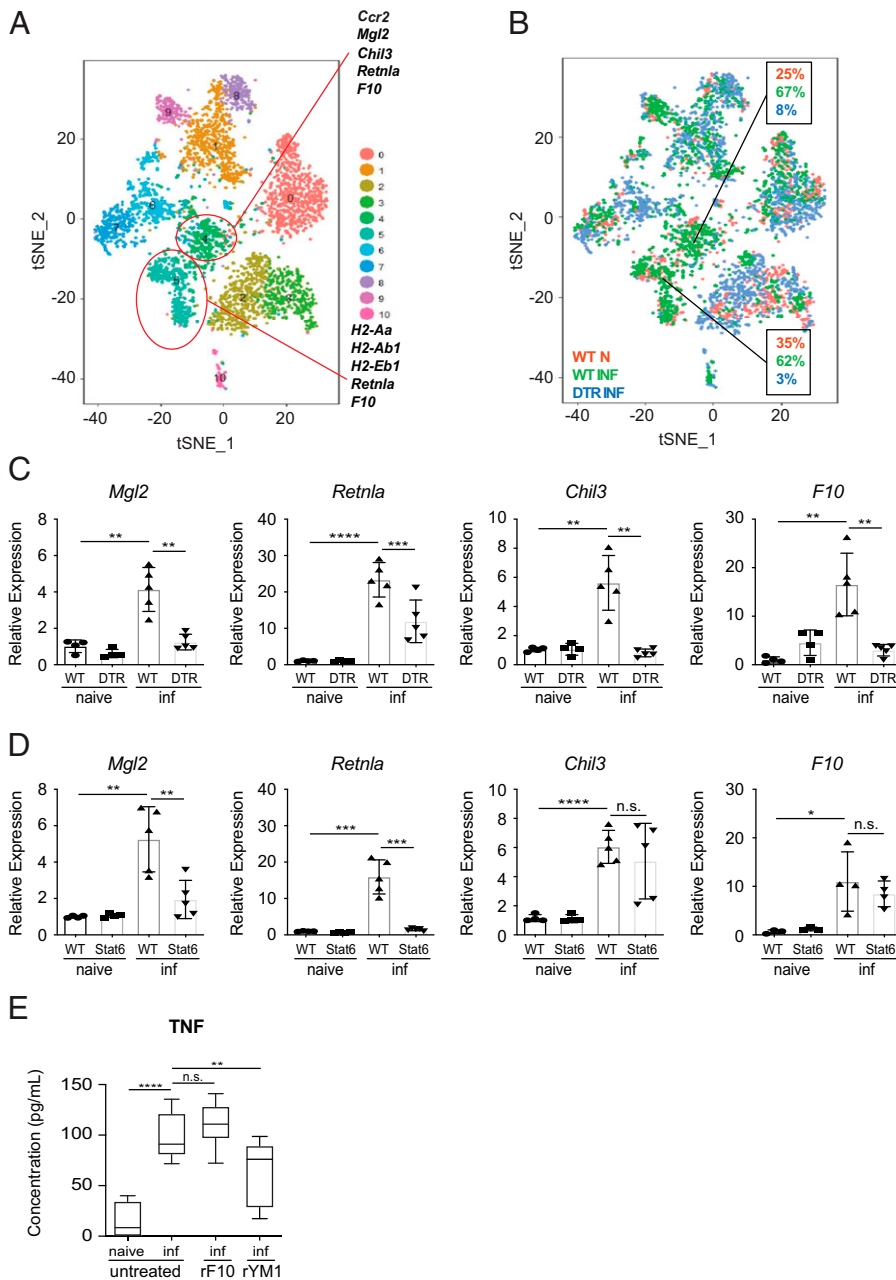

Fig. 5. CCR2$^+$ monocytes and monocyte-derived cells express immunoregulatory factors in the brain following *T. spiralis* infection. Single-cell RNA-seq was performed on sort-purified CD45^{hi} cells, from the brains of naive WT and infected (8 dpi) WT and DTR mice. (*A*) t-SNE dimension reduction illustrating distinct cell populations in the brain. Each group includes CD45^{hi} cells pooled from five mice. (*B*) The relative abundance of each cluster was determined in naive WT, infected WT mice, and infected DTR mice. (*C* and *D*) RNA from whole-brain tissue was extracted from WT, DTR, or STAT6KO mice on 8 dpi and evaluated via RT-qPCR. (*E*) Sort-purified microglia were pooled from naive and infected WT mice. Microglia from infected mice were incubated with rYM1 or rF10 and stimulated. TNF production was evaluated via ELISA. All panels are representative of at least three independent experiments each with at least three biological or technical replicates per group. Statistical analysis was performed using Student's *t* test. *$P < 0.05$; **$P < 0.01$; ***$P < 0.001$; ****$P < 0.0001$; n.s., not significant. Error bars represent SD. Error bars represent ± SD. inf, *T. spiralis*-infected.

ability to inhibit TNF expression (68). Collectively, these data suggest that monocytes and monocyte-derived cells may promote their protective effects via the secretion of these regulatory factors.

To further evaluate this possibility, we sought to determine how the expression of these molecules changed when monocytes were depleted. To accomplish this, we evaluated their expression patterns in our global RNA-seq analysis of whole-brain tissue. Expression of *Mgl2*, *Retnla*, *Chil3*, and *F10* were found to be significantly downregulated in the brain when monocytes were depleted (*SI Appendix*, Table S1, green rows). These results were also confirmed by RT-qPCR analysis of whole-brain tissue (Fig. 5C). It is well established that several of these molecules are highly associated with type 2 cytokine-dependent M2 responses (23, 69). Importantly, our data suggest that the protective functions of monocytes are occurring independently of STAT6-mediated signals (*SI Appendix*, Fig. S1 *E* and *F*). Therefore, we hypothesized that the monocyte-associated molecules responsible for preventing brain inflammation would still be expressed in the brains of infected STAT6KO animals. To test this, we evaluated whether the expression of these markers required STAT6-dependent signaling. While expression levels of *Mgl2* and *Retnla* were significantly reduced in infected STAT6KO mice, *Chil3* and *F10* were found to be unchanged (Fig. 5D). These data strongly suggest that monocytes may promote their protective effects via their production of YM1 (encoded by *Chil3*) and/or F10. To test whether these molecules could regulate microglial activation, we sort-purified and cultured microglia from naive and infected WT mice, thereby removing them from the TNF-suppressive signals found *in vivo*. Importantly, we found that

microglia from infected mice produced significantly more TNF compared to microglia sorted from naive mice (Fig. 5E). Critically, treatment with recombinant YM1 (rYM1), but not recombinant F10 (rF10), significantly reduced TNF production by microglia (Fig. 5E). These data demonstrate that YM1 is sufficient to limit TNF expression by activated microglia and suggest that mechanistically, monocytes regulate neuroinflammation, in part, through their production of YM1.

YM1 Expressing Monocytes Are Sufficient to Prevent Infection-Induced Neuroinflammation. Our studies suggest that infection-induced monocytes are recruited to the brain, where they secrete immunoregulatory factors, such as YM1, that prevent neuroinflammation. To further test this, we evaluated whether brain-resident monocytes exhibit infection-induced increases in YM1 expression. Intracellular staining for YM1 revealed that the percent and total number of YM1-producing monocytes in the brain were significantly increased post-infection (Fig. 6A and *SI Appendix*, Fig. S6 *A* and *B*). Furthermore, the intensity of YM1 expression was also significantly increased as determined by mean fluorescence intensity (Fig. 6B). Similar increases in YM1 were also observed in monocyte-dependent macrophage populations (Fig. 6 *C* and *D* and *SI Appendix*, Fig. S6 *C* and *D*).

Next, we tested whether peripheral monocytes are sufficient to restore YM1 responses and prevent infection-induced neuroinflammation. To test this, we adoptively transferred DTR⁻ CCR2⁺ monocytes from the bone marrow and spleen of infected control mice into *T. spiralis*-infected monocyte-depleted animals. Critically, the adoptive transfer of WT monocytes resulted in a partial restoration of the monocyte compartment in the brain
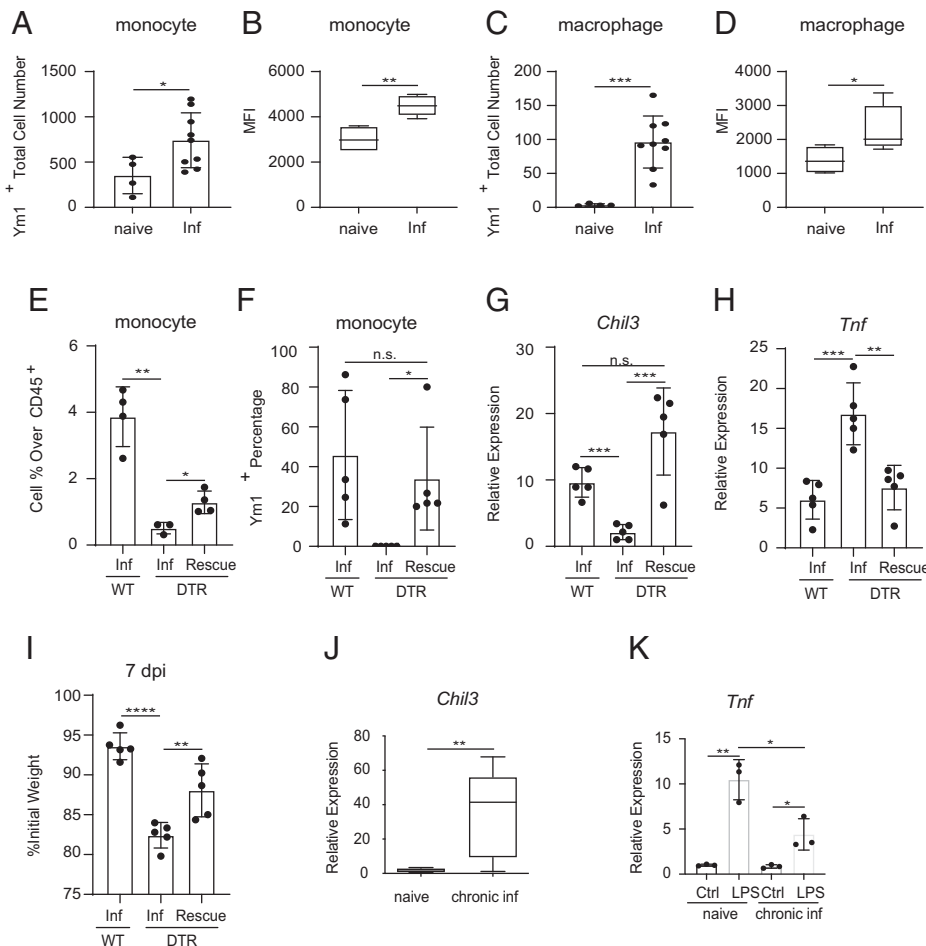

Fig. 6. YM1 expressing monocytes are sufficient to prevent infection-induced neuroinflammation. Intracellular staining of Ym1 in brain (*A* and *B*) monocytes and (*C* and *D*) macrophages from naive and infected WT mice. (*E*) Monocyte percentage over total CD45⁺ cells in brains of infected WT, DTR, and infected DTR mice receiving WT monocytes (Rescue). (*F*) Ym1⁺ monocyte percentage in brains of infected WT, DTR, and infected DTR mice receiving WT monocytes. (*G* and *H*) RNA from whole-brain tissue was extracted from infected WT, DTR, and infected DTR mice receiving WT monocytes, and expression of *Chil3* and *Tnf* were evaluated via RT-qPCR. (*I*) Weights were recorded at the end of the infection. (*J*) RNA from whole-brain tissue was extracted from mice up to 3 months post-infection, and expression of *Chil3* was evaluated via RT-qPCR. (*K*) Infected WT mice were injected with LPS (i.p.) 4 wk post-infection and sacrificed 6 h post-injection. All panels are representative of at least three independent experiments with at least three biological or technical replicates per group per experiment. Statistical analysis was performed using Student's *t* test. *P < 0.05; **P < 0.01; ***P < 0.001; ****P < 0.0001; n.s., not significant. Error bars represent SD. Error bars represent ± SD. inf, *T. spiralis*-infected. MFI, mean fluorescence intensity.

(Fig. 6*E*). Furthermore, intracellular staining confirmed that transferred monocytes produced YM1 at similar levels as those seen in control animals, and their presence was sufficient to restore *Chil3* expression levels in the brain (Fig. 6 *F* and *G*). Finally, monocyte transfer was also sufficient to significantly decrease *TNF* expression and resulted in protection from infection-induced weight loss (Fig. 6 *H* and *I*). Collectively, these data demonstrate that circulating monocytes are recruited to the brain where they promote CNS homeostasis in the context of peripheral inflammation.

Approximately 21 days following *T. spiralis* infection, adult worms are expelled from the intestines, inflammation has resolved, and the parasite begins its latent phase of infection (70). Therefore, we sought to determine whether *Chil3* expression remains increased in the brain after peripheral inflammation is resolved. Importantly, enhanced *Chil3* expression persisted in the brains for up to 3 months post-infection (Fig. 6*J*). These data suggest that infection fundamentally alters the immunologic landscape of the host's brain. Next, we sought to determine if these persistent changes in the CNS correlated with increased protection to subsequent forms of neuroinflammation. To test this, we employed a published protocol of LPS-induced neuroinflammation and evaluated expression of *Tnf* in the brains of infected mice and appropriately age-matched controls. Importantly, previously infected mice exhibited significantly reduced *Tnf* expression in the brain following LPS challenge (Fig. 6*K*). These data demonstrate that *T. spiralis* infection is associated with persistent changes in the brain and increased protection to unrelated forms of neuroinflammation.

Discussion

The CNS is responsible for maintaining homeostatic conditions throughout the body (71, 72). Perhaps not surprisingly, recent studies have begun to reveal that among other systems of the body, the CNS also regulates immunity and inflammation via its effects on the immune system (1, 5, 10, 27, 73). The nervous system is ideally poised to detect invading pathogens via sensory and autonomic neurons that innervate host tissues (3–5, 74). Upon sensing invading pathogens, neurons can initiate reflex circuits that rapidly direct the actions of immune cells. Furthermore, recent work has also defined the capabilities of the nervous system to restrict immune cell activation to prevent undesirable immunopathology (2, 6–8). Included among these reports are studies revealing the existence of an anti-inflammatory reflex that describes the ability of neuron-derived signals to inhibit immune cell production of proinflammatory cytokines, such as TNF, that can become lethal if left unchecked (10, 11, 75). Despite these advances, whether the immune system can act in a similar manner by restricting potentially lethal proinflammatory responses in the CNS remains to be fully defined.

Here we investigated the host-protective roles of monocytes following a *T. spiralis* challenge and demonstrate that mice depleted of CCR2-expressing monocytes suffer from increased infection-induced weight loss and mortality during the early phases of infection. Since these dramatic differences occurred while the parasites were still present in the intestines, we first investigated the importance of monocytes and monocyte-derived macrophages in regulating infection-induced inflammation in the gut. While the loss of monocytes resulted in reduced intestinal M2 responses, monocyte-depleted mice exhibited unremarkable gut pathology, similar worm burdens, and showed no indication of a barrier defect. Collectively, these data suggested that monocyte-depleted mice were not dying as the result of excessive tissue damage caused by the parasitic larvae.

There is a growing appreciation for the involvement of the CNS in regulating peripheral inflammation (1, 10, 27, 28, 75, 76). Studies describing a small subset of patients suffering from neurological symptoms, or neurotrichinosis, indicated that the CNS may be reactive to *T. spiralis*-induced inflammation (52). Therefore, we performed RNA-seq analysis to further investigate whether the CNS is differentially responding to infection in the absence of monocytes. Critically, the brains of *T. spiralis*-infected mice depleted of monocytes exhibited a proinflammatory signature that was characterized by the increased expression of *Tnf*, *Il1b*, *Il6*, and *Il12b*. Furthermore, monocyte-depleted mice crossed to a TNF-deficient background were significantly protected from *T. spiralis*-induced morbidity, indicating that increased expression of proinflammatory cytokines such as TNF in the CNS may play an important role in promoting poor outcomes in the absence of monocytes.

Inflammatory cytokines produced by microglia are reported to promote detrimental neuroinflammation in several disease states, including Alzheimer's and Parkinson's disease (77, 78). Similarly, microglia from *T. spiralis*-infected monocyte-depleted mice expressed elevated levels of cytokines including *Tnf*, *Il1b*, and *Il6*. Consistent with a highly activated state, we found that microglia from monocyte-depleted mice exhibited a reactive phenotype as indicated by changes in IBA1 staining compared to microglia from WT mice. Furthermore, microglia from monocyte-depleted mice also exhibited significantly increased expression of infection-induced *Ccl2*, a monocyte chemoattractant. These data suggest a model by which activated microglia recruit monocytes to the brain, thereby initiating cross-talk that quells proinflammatory cytokine production in the CNS. Consistent with these events, we observed a significant increase in the number of monocytes, macrophages, and dendritic cells in the brains of infected mice compared to naive controls. Importantly, these cells were found to be virtually absent following monocyte depletion. Furthermore, the adoptive transfer of monocytes was sufficient to decrease TNF levels in the brain and prevented morbidity in infected monocyte-depleted hosts. These data further confirm that monocytes are recruited from the periphery to restore CNS homeostasis post-infection.

The studies presented here reveal an important role for infection-induced monocytes and their progeny in preventing neuroinflammation via previously unappreciated cross-talk between the immune system and CNS. Importantly, single-cell RNA-seq studies demonstrate that infection-induced monocytes in the brain share several features with traditional M2 macrophages such as the expression of *Chil3*, which encodes the protein YM1. However, unlike M2 macrophage responses in the intestine, *T. spiralis*-induced expression of *Chil3* in the brain occurred independently of STAT6 signaling, suggesting that *Chil3* expression in this compartment is not dependent on type 2 cytokine signaling. These findings are consistent with a recent report also identifying STAT6-independent expression of *Chil3* in the lung (79). We also demonstrate that rYM1 treatment is sufficient to significantly inhibit TNF expression by activated microglia, suggesting that mechanistically neuroprotective monocytes inhibit brain inflammation, in part, through their expression of this chitinase-like molecule. Finally, we report that *T. spiralis* can induce long-lasting alterations to the immunologic landscape of the host's brain, and that infection can provide protection against subsequent and unrelated forms of neuroinflammation. These data suggest that this neuroprotective pathway remains operational even after peripheral inflammation has been resolved.

While neuroprotective monocytes have been identified in response to ischemic brain injury (80, 81), to the best of our

knowledge, these data are unique in identifying the mobilization and functions of neuroprotective monocytes induced by an infection occurring outside of the CNS. These studies provide substantial insight into the phenotypes of CNS-infiltrating monocytes and suggest that neuroimmune regulatory circuits operate in a bidirectional manner to prevent the induction of life-threatening inflammation from occurring in both the periphery and the CNS. Furthermore, this work indicates that inflammatory responses occurring outside of the CNS can have substantial and persistent effects on the immunologic landscape of the brain that regulates the host's responsiveness to additional forms of neuroinflammation.

Materials and Methods

Mice. C57BL/6 WT (RRID: IMSR_JAX:000664), B6.129S2(C)-Stat6^{tm1Gru}/J (STAT6 KO) (STAT6 KO, RRID: IMSR_JAX:005977), B6(Cg)-Rag2$^{tm1.1Cgn}$/J (RAG2 KO, RRID: IMSR_JAX:008449), and B6.129S-Tnf^{tm1Gkl}/J (TNF KO, RRID: IMSR_JAX:005540) were purchased from The Jackson Laboratory. CCR2-DTR and CCR2-GFP mice on a C57BL/6 background were generously provided by A.R., Rutgers University, New Brunswick, NJ. Male and female age-matched mice were used for all experiments. Mice were housed socially (three to five mice per cage) on a 12-h light/dark cycle in individually ventilated cages, and with *ad libitum* access to food and water. Mice were maintained in specific pathogen-free facilities at the Rutgers New Jersey Medical School. All protocols were approved by the Rutgers Institutional Animal Care and Use Committee (protocol nos. 00017, 17025, or 16045).

***T. spiralis* Infection, LPS Injection, Cell Depletion, and Adoptive Transfer.** Methods for maintenance, recovery, infection, and isolation of *T. spiralis* larvae were performed as previously described (82). All strains of mice were infected with 500 *T. spiralis* muscle larvae by oral gavage and harvested 8 dpi or 90 dpi for chronic infection. Weight was carefully monitored and recorded, and any mouse that lost >20% of their initial weight was sacrificed. For LPS-challenge, LPS was injected 4 wk post-infection, while animals were sacrificed 6 h post-LPS injection.

For depletion of CCR2$^+$ monocytes, CCR2-DTR mice and littermate controls were handled as published previously (34). The generalized depletion of macrophages and other phagocytic cells were executed based on the protocol from Liposoma. At necropsy, single-cell suspensions of mesenteric lymph nodes and spleens, and intestinal worm counts were processed as previously described (83). Whole blood was collected in BD Vacutainer Glass Blood Collection Tubes with K3 EDTA, and plasma was isolated for later analysis. Sections of brain, small intestine, kidney, liver, and gastrocnemius muscle were collected in RNAlater buffer for RT-qPCR analysis and formalin for histological analysis (H&E) and immunofluorescent microscopy. ImageJ (v1.52a) software was used to measure cross-sectional areas of muscle fibers in the gastrocnemius (84).

For the adoptive transfer of monocytes to monocyte-depleted animals, monocytes were isolated from infected WT mice bone marrow and spleen 2, 3, 4, 5, and 6 dpi, and then sort-purified. One to one and a half million cells were given to each DTR recipient through retro-orbital vein intravenous injection. Control animals received same volume of sterile PBS.

Flow Cytometry and Cell Sorting. Cells were stained with monoclonal anti-mouse fluorescently-conjugated antibodies: F4/80 (T45-2342), CD3 (145-2C11; BD Biosciences), CD19 (1D3; BioLegend), CD11b (MI/70; BD Biosciences), CD11c (HL3; BD Biosciences), Ly6C (HK1.4; eBio), Ly6G (1A8; BD Biosciences), MHCII (M5/114.15.2; BioLegend), IgE (23G3; eBio), CD45 (30-F11; BD Biosciences), and CD68 (Y1/82A; eBio). To block nonspecific Fc receptor binding, cells were incubated with rat anti-mouse CD16/CD32 (BD Biosciences) for 10 min prior to staining. DAPI (Thermo Fisher Scientific) was added prior to acquisition to identify live cells. Monocytes were analyzed as CD45^{hi}Ly6C$^+$CD11b$^+$Ly6G$^-$ MHCII$^-$CD11c$^-$ cells, macrophages were analyzed as CD45^{hi}CD11b$^+$MHCII$^+$Ly6G$^-$CD11c$^-$ or CD45^{hi}CD11b$^+$F4/80$^+$Ly6G$^-$CD11c$^-$, dendritic cells were analyzed as CD45^{hi} CD11b$^+$CD11c$^+$MHCII$^+$Ly6G$^-$, microglia were analyzed as CD45^{mid}CD11b$^+$ cells. Samples were acquired on a Fortessa X-20 flow cytometer (BD Biosciences) and analyzed using FlowJo software (v10.0.5, Tree Star). Cell sorting was performed

using a FACS Aria II cell sorter or FACS Aria Fusion (BD Biosciences). Microglia were sort-purified as CD45^{mid}CD11b$^+$ cells; hematopoietic cells were sort-purified as CD45^{hi} cells.

Post-surface staining, cells undergoing intracellular staining were placed in fixation buffer (eBioscience) for 10 min, and then permeabilized in permeabilization buffer (eBioscience) for 1 h. Cells were incubated with biotinylated goat anti-mouse chitinase 3-like 3/ECF-L (Ym1, R&D Systems) for 1 h, and then with secondary antibody attached to streptavidin for 1 h.

Isolation of Lamina Propria Cells of the Gut. After removal of the Peyer's patches, the small intestine was cut longitudinally and thoroughly washed in ice-cold HBSS. The intestine was cut into ∼1-cm pieces and incubated in pre-warmed predigestion solution (2 mM EDTA, 5% FBS, 1 mM DTT in HBSS) for 20 min at 37 °C. The sample was filtered through a 100-μm cell strainer and flow-through was discarded. Small intestine was collected and incubated in prewarmed (37 °C) digestion solution (5% FBS, 0.25 mg/mL DNase I [Roche], 0.1 mg/mL collagenase D [Roche]) for 10 min at 37 °C. The sample was filtered through a 40-μm cell strainer, and flow-through was collected and immediately spun at 500 × g for 10 min at room temperature. After centrifugation, supernatant was discarded, and the pellet was resuspended in HBSS with 5% FBS. The digestion step was repeated two to three more times. Lamina propria cells from all digestions were combined and then centrifuged at 500 × g for 10 min at room temperature. The pellet was resuspended in 2 mL of 20% Percoll (GE Healthcare; diluted in HBSS) and transferred into a 15-mL conical tube. 2 mL of 40%, and then 2 mL of 80% Percoll were underlaid to form a density gradient. The sample was centrifuged in a swinging bucket rotor at room temperature at 600 × g for 20 min with deceleration off. Cells were pipetted off the 40/80 interface to a new 15-mL conical tube and then filled to the top with HBSS. The sample was centrifuged for 5 min at 600 × g at 4 °C and the supernatant was discarded. The pellet was resuspended in staining solution for flow cytometry.

Isolation of Immune Cells from the Brain. Immune cells were isolated from the brain as previously described (34). Following Percoll gradient steps and wash of the pellet with 1 mL of FACS buffer, the pellet was resuspended in 50 μL of Fc block (1:100 in FACS buffer) and incubated on ice for 15 min. Afterward, 50 μL of antibody staining solution was added, and samples were incubated for 30 more minutes. Samples were washed, spun at 10,000 × g for 1 min, resuspended in FACS buffer, and acquired.

RNA Isolation and RT-qPCR Analysis. RNA from the small intestine, brain, liver, and kidney were isolated by homogenization in TRIzol (Thermo Fisher Scientific) followed by phenol-chloroform extraction and isopropanol precipitation. The resulting RNA was purified using the RNA clean-up protocol from Qiagen's RNeasy Mini Kit. RNA from the gastrocnemius muscle was extracted via Qiagen's RNeasy Fibrous Tissue Mini Kit. Extracted cDNA was generated per standard protocol with SuperScript reverse transcriptase (Thermo Fisher Scientific) and used as input for qPCR. Real-time data were analyzed using the ΔΔCT method using SYBR Green chemistry (Applied Biosystems) with β-actin (Actb) serving as the endogenous housekeeping gene. Samples were normalized to naive controls. The following QuantiTech primer assays from Qiagen were used (see Supporting Information for catalog numbers): Actb, Tnf, Il1b, Il6, Il12b, Il18, Arg1, Retnla, Chil3, Ccl2, Havcr1, Crp, Mgl2, F10, Foxo1, Fbxo32, Trim63, and iNOS.

T Cell Stimulations and ELISAs. Single-cell suspensions were made from mesenteric lymph nodes. Cells were cultured in RPMI complete medium and treated with or without anti-CD3 (clone 145-2C11; BD Biosciences) and anti-CD28 antibodies (clone 37.51; BD Biosciences) for 72 h. Standard sandwich ELISA was performed to measure IL-4 (clones 11B11 and BVD6-24G2) levels in the cell-free supernatants. Plasma quantities of IgE (BD Biosciences), leptin (Thermo Fisher Scientific), ghrelin (Sigma-Aldrich), alanine transaminase (Sigma-Aldrich), creatine kinase (Sigma-Aldrich), endotoxin (Pierce Biotech), and Crp (Abcam) were measured by commercial ELISA kits.

Microglia Stimulation. Microglia were isolated from the brains of naive or *T. spiralis*-infected (8 dpi) WT mice via cell sorting (CD45^{mid}CD11b$^+$ cells). Microglia (25,000 per well) were cultured in 150 μL of RPMI complete tissue culture media. Microglia isolated from infected mice were incubated with 40 nM

recombinant F10 or 1 μg/mL recombinant YM1 (37 °C, 5% CO_2) for 5 h. Afterward, all microglial cultures were stimulated with PMA (50 ng/mL) and ionomycin (500 ng/mL) for another 5 h. Supernatants were collected, and the production of TNF was evaluated via ELISA (Thermo Fisher Scientific).

Immunofluorescent Staining. Unstained sections cut from paraffin-embedded brain tissue were deparaffinized and rehydrated by washing three times with xylene, once with 100% ethanol, once with 95% ethanol, once with 70% ethanol, and then once with ddH$_2$O. Antigen retrieval was accomplished by microwave heating the sections in 10 mM of citric acid buffer (pH 6.0). Sections were blocked with goat serum (Vector Labs) for 1 h at room temperature. Afterward, sections were treated with Fc block (BD Biosciences) diluted in normal goat serum (1:100) for 10 min at room temperature. Primary antibody (IBA1; Thermo Fisher Scientific) or the appropriate isotype control (diluted in goat serum, 1:200) was then added followed by incubation in a humidifying chamber overnight at 4 °C. The following day, sections were covered with biotinylated secondary antibody (diluted in goat serum, 1:200; Vector Labs) for 2 h at room temperature, followed by incubation with Fluorescein Avidin DCS (diluted in Hepes buffer, 1:400; Vector Labs) for 10 min at room temperature. Coverslips were applied to the slides using Vectashield mounting media with DAPI. Slides were incubated overnight in the dark at 4 °C and analyzed the next day. Images were taken using a Leica DM6000B microscope and Leica Application Suite Advanced Fluorescence software.

RNA-seq. Total cellular RNA was extracted using TRIzol reagent according to the manufacturer's instructions (Thermo Fisher Scientific). The quality of RNA was first checked for integrity on an Agilent Bioanalyzer 2100; samples with an RNA integrity number (RIN) >7.0 were used for subsequent processing. Total RNA was subjected to two rounds of poly(A) selection using oligo-d(T)25 magnetic beads (New England Biolabs). The Illumina compatible RNA-seq library was prepared using New England Biolabs next ultra RNA-seq library preparation kit. The cDNA libraries were purified using AmpureXP beads and quantified on an Agilent Bioanalyzer and qubit analysis. Equimolar amounts of barcoded libraries were pooled and sequenced on Illumina NextSEq. 500 platform (Illumina) with 1 × 75 configuration.

CLC Genomics Workbench v11.0.1 (Qiagen) was used for RNA-seq analysis. Demultiplexed fastq files from an RNA-seq libraries were imported into the CLC software. Bases with low quality were trimmed and reads were mapped to reference genome *Mus musculus* genome GRCm38. The reference genome sequence and annotation files were downloaded from ENSEMBL, release.92 (Mus_musculus.GRCm38.92.fa, and Mus_musculus.GRCm38.92.gtf). The aligned reads were obtained using the RNA-Seq Analysis Tool of CLC Genomics Workbench. Statistical analysis of differentially expressed genes was carried out based on a negative binomial model (85) using the standard tools within the CLC Genomic Workbench. Replicates were averaged, differentially expressed significant genes with a false-discovery rate (FDR) $P < 0.05$ and fold-change (FC) of an absolute value $> 1.5/< -1.5$ was used as the cutoff for analysis.

Up-regulated and down-regulated genes were analyzed through GSEA (v4.0.3) to identify enriched pathways.

Single-Cell RNA-seq. Cells isolated from the whole brains of naive WT, infected WT, and infected CCR2-DTR mice were sort-purified on live CD45^{hi} cells from five biological replicates and pooled. Sort-purified cells were then processed using the 10X Genomics Chromium Controller. Cell suspensions were loaded onto the Chromium Single Cell A Chip for cell lysis and barcoding. RNA from individual cells was reverse transcribed and sequencing libraries prepared using the Chromium Single Cell 3′ Library Kit v2 following the manufacturer's protocol. Samples were sequenced using an Illumina NextSEq. 550 with standard 10X Genomics Configuration (26 bp × 98 bp). After sequencing, raw bcl files were processed using the cellranger mkfastq command for sample demultiplexing and conversion to .fastq files, followed by cellranger count for cell barcode and UMI deconvolution as well as mapping to the respective reference genome. Processed digital gene-expression matrices were imported into R studio for analysis using the Seurat package. Samples were aligned along common sources of variation and compared using canonical correlation analysis to identify unique clusters of cells within the samples. Marker genes for each sample and cluster were identified and used for generation of downstream plots within the Seurat package. All packages are maintained to be best in class and are regularly updated to their most recent release.

Statistics. Results are shown as mean ± SD. Statistical analysis was performed using Student's *t* tests in Prism (v6.07; GraphPad Software).

Author affiliations: ªCenter for Immunity and Inflammation, New Jersey Medical School, Rutgers, The State University of New Jersey, Newark, NJ 07103; ᵇDepartment of Medicine, New Jersey Medical School, Rutgers, The State University of New Jersey, Newark, NJ 07103; ᶜDepartment of Pathology, Immunology, and Laboratory Medicine, New Jersey Medical School, Rutgers, The State University of New Jersey, Newark, NJ 07103; ᵈDepartment of Pediatrics, New Jersey Medical School, Rutgers, The State University of New Jersey, Newark, NJ 07103; and ᵉDepartment of Microbiology, Biochemistry, and Molecular Genetics, New Jersey Medical School, Rutgers, The State University of New Jersey, Newark, NJ 07103

1. S. Ibiza *et al.*, Glial-cell-derived neuroregulators control type 3 innate lymphoid cells and gut defence. *Nature* **535**, 440–443 (2016).
2. H. Nagashima *et al.*, Neuropeptide CGRP limits group 2 innate lymphoid cell responses and constrains type 2 inflammation. *Immunity* **51**, 682–695.e6 (2019).
3. N. Y. Lai *et al.*, Gut-innervating nociceptor neurons regulate Peyer's patch microfold cells and SFB levels to mediate salmonella host defense. *Cell* **180**, 33–49.e22 (2020).
4. I. M. Chiu *et al.*, Bacteria activate sensory neurons that modulate pain and inflammation. *Nature* **501**, 52–57 (2013).
5. P. Baral *et al.*, Nociceptor sensory neurons suppress neutrophil and γδ T cell responses in bacterial lung infections and lethal pneumonia. *Nat. Med.* **24**, 417–426 (2018).
6. J. M. Inclan-Rico *et al.*, Basophils prime group 2 innate lymphoid cells for neuropeptide-mediated inhibition. *Nat. Immunol.* **21**, 1181–1193 (2020).
7. O. O. Oyesola *et al.*, PGD2 and CRTH2 counteract Type 2 cytokine-elicited intestinal epithelial responses during helminth infection. *J. Exp. Med.* **218**, e20202178 (2021).
8. S. Moriyama *et al.*, β₂-adrenergic receptor-mediated negative regulation of group 2 innate lymphoid cell responses. *Science* **359**, 1056–1061 (2018).
9. C. Chu *et al.*, The ChAT-acetylcholine pathway promotes group 2 innate lymphoid cell responses and anti-helminth immunity. *Sci. Immunol.* **6**, eabe3218 (2021).
10. V. A. Pavlov, S. S. Chavan, K. J. Tracey, Molecular and functional neuroscience in immunity. *Annu. Rev. Immunol.* **36**, 783–812 (2018).
11. H. Wang *et al.*, Nicotinic acetylcholine receptor alpha7 subunit is an essential regulator of inflammation. *Nature* **421**, 384–388 (2003).
12. J. E. Allen, R. M. Maizels, Diversity and dialogue in immunity to helminths. *Nat. Rev. Immunol.* **11**, 375–388 (2011).
13. R. M. Anthony, L. I. Rutitzky, J. F. Urban Jr, M. J. Stadecker, W. C. Gause, Protective immune mechanisms in helminth infection. *Nat. Rev. Immunol.* **7**, 975–987 (2007).
14. E. Pozio, The broad spectrum of Trichinella hosts: From cold- to warm-blooded animals. *Vet. Parasitol.* **132**, 3–11 (2005).
15. E. Pozio, New patterns of Trichinella infection. *Vet. Parasitol.* **98**, 133–148 (2001).
16. U. de Boni, M. M. Lenczner, J. W. Scott, Autopsy of an Egyptian mummy. 6. Trichinella spiralic cyst. *Can. Med. Assoc. J.* **117**, 472–472 (1977).
17. E. P. Hoberg, K. E. Galbreath, J. A. Cook, S. J. Kutz, L. Polley, "Northern host–parasite assemblages: History and biogeography on the borderlands of episodic climate and environmental transition" in *Advances in Parasitology*, D. Rollinson, S. I. Hay, Eds. (Academic Press, 2012), vol. 79, chap. 1, pp. 1–97.
18. S. A. Babayan *et al.*, The immune and non-immune pathways that drive chronic gastrointestinal helminth burdens in the wild. *Front. Immunol.* **9**, 56 (2018).
19. I. L. King, Y. Li, Host-parasite interactions promote disease tolerance to intestinal helminth infection. *Front. Immunol.* **9**, 2128 (2018).
20. R. M. Maizels, M. Yazdanbakhsh, Immune regulation by helminth parasites: Cellular and molecular mechanisms. *Nat. Rev. Immunol.* **3**, 733–744 (2003).
21. W. C. Gause, T. A. Wynn, J. E. Allen, Type 2 immunity and wound healing: Evolutionary refinement of adaptive immunity by helminths. *Nat. Rev. Immunol.* **13**, 607–614 (2013).
22. F. Chen *et al.*, An essential role for TH2-type responses in limiting acute tissue damage during experimental helminth infection. *Nat. Med.* **18**, 260–266 (2012).
23. F. Chen *et al.*, Neutrophils prime a long-lived effector macrophage phenotype that mediates accelerated helminth expulsion. *Nat. Med.* **15**, 938–946 (2014).
24. T. Kreider, R. M. Anthony, J. F. Urban Jr, W. C. Gause, Alternatively activated macrophages in helminth infections. *Curr. Opin. Immunol.* **19**, 448–453 (2007).

25. D. Rückerl, J. E. Allen, Macrophage proliferation, provenance, and plasticity in macroparasite infection. *Immunol. Rev.* **262**, 113–133 (2014).

26. F. Chen *et al.*, Helminth resistance is mediated by differential activation of recruited monocyte-derived alveolar macrophages and arginine depletion. *Cell Rep.* **38**, 110215 (2022).

27. C. Chu, D. Artis, I. M. Chiu, Neuro-immune interactions in the tissues. *Immunity* **52**, 464–474 (2020).

28. C. S. N. Klose, H. Veiga-Fernandes, Neuroimmune interactions in peripheral tissues. *Eur. J. Immunol.* **51**, 1602–1614 (2021).

29. N. van Rooijen, E. Hendrikx, Liposomes for specific depletion of macrophages from organs and tissues. *Methods Mol. Biol.* **605**, 189–203 (2010).

30. C. C. Bain *et al.*, Resident and pro-inflammatory macrophages in the colon represent alternative context-dependent fates of the same Ly6Chi monocyte precursors. *Mucosal Immunol.* **6**, 498–510 (2013).

31. C. Shi, E. G. Pamer, Monocyte recruitment during infection and inflammation. *Nat. Rev. Immunol.* **11**, 762–774 (2011).

32. A. T. Satpathy *et al.*, Notch2-dependent classical dendritic cells orchestrate intestinal immunity to attaching-and-effacing bacterial pathogens. *Nat. Immunol.* **14**, 937–948 (2013).

33. Z. Li, X. Xu, X. Feng, P. M. Murphy, The macrophage-depleting agent clodronate promotes durable hematopoietic chimerism and donor-specific skin allograft tolerance in mice. *Sci. Rep.* **6**, 22143 (2016).

34. T. M. Hohl *et al.*, Inflammatory monocytes facilitate adaptive CD4 T cell responses during respiratory fungal infection. *Cell Host Microbe* **6**, 470–481 (2009).

35. O. Atochina, T. Daly-Engel, D. Piskorska, E. McGuire, D. A. Harn, A schistosome-expressed immunomodulatory glycoconjugate expands peritoneal Gr1(+) macrophages that suppress naive CD4(+) T cell proliferation via an IFN-gamma and nitric oxide-dependent mechanism. *J. Immunol.* **167**, 4293–4302 (2001).

36. L. Brys *et al.*, Reactive oxygen species and 12/15-lipoxygenase contribute to the antiproliferative capacity of alternatively activated myeloid cells elicited during helminth infection. *J. Immunol.* **174**, 6095–6104 (2005).

37. J. J. Reece, M. C. Siracusa, A. L. Scott, Innate immune responses to lung-stage helminth infection induce alternatively activated alveolar macrophages. *Infect. Immun.* **74**, 4970–4981 (2006).

38. R. M. Anthony *et al.*, Memory T(H)2 cells induce alternatively activated macrophages to mediate protection against nematode parasites. *Nat. Med.* **12**, 955–960 (2006).

39. M. Morimoto *et al.*, Peripheral CD4 T cells rapidly accumulate at the host: Parasite interface during an inflammatory Th2 memory response. *J. Immunol.* **172**, 2424–2430 (2004).

40. Z. Liu *et al.*, IL-2 and autocrine IL-4 drive the in vivo development of antigen-specific Th2 T cells elicited by nematode parasites. *J. Immunol.* **174**, 2242–2249 (2005).

41. M. H. Kaplan, U. Schindler, S. T. Smiley, M. J. Grusby, Stat6 is required for mediating responses to IL-4 and for development of Th2 cells. *Immunity* **4**, 313–319 (1996).

42. C. O. S. Souza, L. G. Gardinassi, V. Rodrigues, L. H. Faccioli, Monocyte and macrophage-mediated pathology and protective immunity during schistosomiasis. *Front. Microbiol.* **11**, 1973 (2020).

43. W. C. Gause, C. Rothlin, P. Loke, Heterogeneity in the initiation, development and function of type 2 immunity. *Nat. Rev. Immunol.* **20**, 603–614 (2020).

44. C. Campbell, A. Rudensky, Roles of regulatory T cells in tissue pathophysiology and metabolism. *Cell Metab.* **31**, 18–25 (2020).

45. J. Li, J. Tan, M. M. Martino, K. O. Lui, Regulatory T-cells: Potential regulator of tissue repair and regeneration. *Front. Immunol.* **9**, 585 (2018).

46. D. R. Herbert, T. Orekov, C. Perkins, F. D. Finkelman, IL-10 and TGF-beta redundantly protect against severe liver injury and mortality during acute schistosomiasis. *J. Immunol.* **181**, 7214–7220 (2008).

47. G. M. Chertow, E. Burdick, M. Honour, J. V. Bonventre, D. W. Bates, Acute kidney injury, mortality, length of stay, and costs in hospitalized patients. *J. Am. Soc. Nephrol.* **16**, 3365–3370 (2005).

48. R. G. Molloy, J. A. Mannick, M. L. Rodrick, Cytokines, sepsis and immunomodulation. *Br. J. Surg.* **80**, 289–297 (1993).

49. H. Fukui, Relation of endotoxin, endotoxin binding proteins and macrophages to severe alcoholic liver injury and multiple organ failure. *Alcohol. Clin. Exp. Res.* **29** (11, suppl.) 172S–179S (2005).

50. L. Ma *et al.*, The acute liver injury in mice caused by nano-anatase TiO$_2$. *Nanoscale Res. Lett.* **4**, 1275–1285 (2009).

51. T. Komada *et al.*, Role of NLRP3 inflammasomes for rhabdomyolysis-induced acute kidney injury. *Sci. Rep.* **5**, 10901 (2015).

52. S. Nikolić *et al.*, [Neurologic manifestations in trichinosis.] [in Serbian] *Srp. Arh. Celok. Lek.* **126**, 209–213 (1998).

53. C. M. Ribeiro *et al.*, Tumor necrosis factor alpha (TNF-α) and its soluble receptors are associated with disability, disability progression and clinical forms of multiple sclerosis. *Inflamm. Res.* **68**, 1049–1059 (2019).

54. E. Paouri, O. Tzara, S. Zenelak, S. Georgopoulos, Genetic deletion of tumor necrosis factor-α attenuates amyloid-β production and decreases amyloid plaque formation and glial response in the 5XFAD model of Alzheimer's disease. *J. Alzheimers Dis.* **60**, 165–181 (2017).

55. M. N. Karpenko *et al.*, Interleukin-1β, interleukin-1 receptor antagonist, interleukin-6, interleukin-10, and tumor necrosis factor-α levels in CSF and serum in relation to the clinical diversity of Parkinson's disease. *Cell. Immunol.* **327**, 77–82 (2018).

56. D. G. Brohawn, L. C. O'Brien, J. P. Bennett Jr., RNAseq analyses identify tumor necrosis factor-mediated inflammation as a major abnormality in ALS spinal cord. *PLoS One* **11**, e0160520 (2016).

57. T. P. Braun *et al.*, Central nervous system inflammation induces muscle atrophy via activation of the hypothalamic-pituitary-adrenal axis. *J. Exp. Med.* **208**, 2449–2463 (2011).

58. M. Pasparakis, L. Alexopoulou, V. Episkopou, G. Kollias, Immune and inflammatory responses in TNF alpha-deficient mice: A critical requirement for TNF alpha in the formation of primary B cell follicles, follicular dendritic cell networks and germinal centers, and in the maturation of the humoral immune response. *J. Exp. Med.* **184**, 1397–1411 (1996).

59. M. E. Lull, M. L. Block, Microglial activation and chronic neurodegeneration. *Neurotherapeutics* **7**, 354–365 (2010).

60. R. Orihuela, C. A. McPherson, G. J. Harry, Microglial M1/M2 polarization and metabolic states. *Br. J. Pharmacol.* **173**, 649–665 (2016).

61. Y. Tang, W. Le, Differential roles of M1 and M2 microglia in neurodegenerative diseases. *Mol. Neurobiol.* **53**, 1181–1194 (2016).

62. L. Carniglia *et al.*, Neuropeptides and microglial activation in inflammation, pain, and neurodegenerative diseases. *Mediators Inflamm.* **2017**, 5048616–5048616 (2017).

63. A. Yamashita, Y. Hatazawa, Y. Hirose, Y. Ono, Y. Kamei, FOXO1 delays skeletal muscle regeneration and suppresses myoblast proliferation. *Biosci. Biotechnol. Biochem.* **80**, 1531–1535 (2016).

64. P. Bonaldo, M. Sandri, Cellular and molecular mechanisms of muscle atrophy. *Dis. Model. Mech.* **6**, 25–39 (2013).

65. C. D'Mello, T. Le, M. G. Swain, Cerebral microglia recruit monocytes into the brain in response to tumor necrosis factoralpha signaling during peripheral organ inflammation. *J. Neurosci.* **29**, 2089–2102 (2009).

66. Y. Kumamoto *et al.*, CD301b$^+$ dermal dendritic cells drive T helper 2 cell-mediated immunity. *Immunity* **39**, 733–743 (2013).

67. L. C. Osborne *et al.*, Coinfection. Virus-helminth coinfection reveals a microbiota-independent mechanism of immunomodulation. *Science* **345**, 578–582 (2014).

68. E. M. Gleeson *et al.*, Activated factor X signaling via protease-activated receptor 2 suppresses pro-inflammatory cytokine production from lipopolysaccharide-stimulated myeloid cells. *Haematologica* **99**, 185–193 (2014).

69. M. G. Nair, D. W. Cochrane, J. E. Allen, Macrophages in chronic type 2 inflammation have a novel phenotype characterized by the abundant expression of Ym1 and Fizz1 that can be partly replicated in vitro. *Immunol. Lett.* **85**, 173–180 (2003).

70. M. Mitreva, D. P. Jasmer, "Biology and genome of *Trichinella spiralis*," J. Hodgkin, Ed., in *WormBook*, http://www.wormbook.org/chapters/www_genomesTrichinella/genomesTrichinella.html. (The *C. elegans* Research Community, WormBook, 2006). Accessed 26 August 2022.

71. M. G. Myers, Jr, A. H. Affinati, N. Richardson, M. W. Schwartz, Central nervous system regulation of organismal energy and glucose homeostasis. *Nat. Metab.* **3**, 737–750 (2021).

72. C. L. Tan, Z. A. Knight, Regulation of body temperature by the nervous system. *Neuron* **98**, 31–48 (2018).

73. E. E. Jean, O. Good, J. M. I. Rico, H. L. Rossi, D. R. Herbert, Neuroimmune regulatory networks of the airway mucosa in allergic inflammatory disease. *J. Leukoc. Biol.* **111**, 209–221 (2022).

74. J. A. Cohen *et al.*, Cutaneous TRPV1$^+$ neurons trigger protective innate type 17 anticipatory immunity. *Cell* **178**, 919–932.e14 (2019).

75. U. Andersson, K. J. Tracey, Reflex principles of immunological homeostasis. *Annu. Rev. Immunol.* **30**, 313–335 (2012).

76. D. Sharma, J. D. Farrar, Adrenergic regulation of immune cell function and inflammation. *Semin. Immunopathol.* **42**, 709–717 (2020).

77. M. T. Heneka *et al.*, Neuroinflammation in Alzheimer's disease. *Lancet Neurol.* **14**, 388–405 (2015).

78. S. G. Daniele *et al.*, Activation of MyD88-dependent TLR1/2 signaling by misfolded α-synuclein, a protein linked to neurodegenerative disorders. *Sci. Signal.* **8**, ra45 (2015).

79. F. R. Svedberg *et al.*, The lung environment controls alveolar macrophage metabolism and responsiveness in type 2 inflammation. *Nat. Immunol.* **20**, 571–580 (2019).

80. L. Garcia-Bonilla *et al.*, Endogenous protection from ischemic brain injury by preconditioned monocytes. *J. Neurosci.* **38**, 6722–6736 (2018).

81. J. Pedragosa *et al.*, CCR2 deficiency in monocytes impairs angiogenesis and functional recovery after ischemic stroke in mice. *J. Cereb. Blood Flow Metab.* **40** (1_suppl), S98–S116 (2020).

82. J. F. Urban Jr *et al.*, Stat6 signaling promotes protective immunity against Trichinella spiralis through a mast cell- and T cell-dependent mechanism. *J. Immunol.* **164**, 2046–2052 (2000).

83. P. R. Giacomin *et al.*, Thymic stromal lymphopoietin-dependent basophils promote Th2 cytokine responses following intestinal helminth infection. *J. Immunol.* **189**, 4371–4378 (2012).

84. C. A. Schneider, W. S. Rasband, K. W. Eliceiri, NIH Image to ImageJ: 25 years of image analysis. *Nat. Methods* **9**, 671–675 (2012).

85. M. D. Robinson, D. J. McCarthy, G. K. Smyth, edgeR: A Bioconductor package for differential expression analysis of digital gene expression data. *Bioinformatics* **26**, 139–140 (2010).

86. C. B. Sy, M. C. Siracusa, Next-Generation Sequencing Facilitates Quantitative Analysis of Wild Type and Monocyte-Depleted Brain Transcriptomes. NCBI. https://www.ncbi.nlm.nih.gov/geo/query/acc.cgi?acc=GSE190493. Accessed 25 August 2022.

87. C. B. Sy, M. C. Siracusa, Next Generation Sequencing Facilitates Single Cell Analysis of Wild Type and Monocyte-Depleted Brain Transcriptomes. NCBI. https://www.ncbi.nlm.nih.gov/geo/query/acc.cgi?acc=GSE189957. Accessed 25 August 2022.